Argon assisted chemical vapor deposition of CrO_2: An efficient process leading to high quality epitaxial films

A.C. Duarte [a, b], N. Franco [c], A.S. Viana [d], N.I. Polushkin [a, b], A.J. Silvestre [b, e], O. Conde [a, b, *]

[a] Departamento de Física, Faculdade de Ciências, Universidade de Lisboa, 1749-016 Lisboa, Portugal
[b] Centro de Física e Engenharia de Materiais Avançados (CeFEMA), 1049-001 Lisboa, Portugal
[c] Centro de Ciências e Tecnologias Nucleares, IST, Universidade de Lisboa, 2695-066 Bobadela, Portugal
[d] Centro de Química e Bioquímica, Faculdade de Ciências, Universidade de Lisboa, 1749-016 Lisboa, Portugal
[e] Área Departamental de Física, ISEL – Instituto Superior de Engenharia de Lisboa, Instituto Politécnico de Lisboa, 1959-007 Lisboa, Portugal

ARTICLE INFO

ABSTRACT

A comparative study of the structural, microstructural and magnetic properties of CrO_2 thin films grown onto (110) and (100) TiO_2 rutile single crystal substrates by chemical vapor deposition (CVD), using CrO_3 as chromium precursor and either oxygen or argon as carrier gas is presented. Our results show that growth under argon carrier gas leads to high quality CrO_2 epilayers with structural and magnetic properties similar to those obtained using the more standard oxygen carrier gas. Furthermore, we interpret the larger magnetic coercivity observed for the (110) oriented films in terms of their microstructure, in particular of the highest strain and edge roughness of the building structures of the CrO_2 epilayers, which are settled by the substrate crystallographic orientation.

© 2016 Elsevier B.V. All rights reserved.

1. Introduction

CrO_2 is a material of choice for spintronics. It has been extensively studied by the scientific community [1–12] since the pioneering work carried out in the 60's of last century as reviewed in Ref. [13]. Recent findings such as the spin triplet supercurrents [14–17], the coexistence of universal and topological anomalous Hall effects and the robustness of spin polarization up to room temperature [18] have strongly contributed to keep alive, or even increase, the interest on potentially using CrO_2 thin films in spintronic and magnonic devices [19–22]. But the studies on chromium dioxide have not been limited to fundamental or applied science. Indeed, CrO_2 has been used in industry covering a wide range of applications *e.g.* audio, video, instrumentation and computer technology due to its exceptional properties as a magnetic storage material [13].

Although some attempts have been pursued to grow thin films of the single CrO_2 compound by physical vapor deposition methods

[23–25], only chemical vapor deposition (CVD) has shown to lead to high quality CrO_2 layers [26–30]. CrO_2 epitaxial layers are currently grown on TiO_2 rutile phase and sapphire substrates by CVD using CrO_3 as the chromium precursor, which is carried out into the reaction zone by an oxygen flux. While chromium precursors other than CrO_3, *e.g.* Cr_8O_{21} [31] and CrO_2Cl_2 [8,10], have also been used in the CVD of CrO_2 yielding films with similar properties, the use of an oxygen flux has been pointed out as critical for the overall CrO_2 synthesis process. To our knowledge, only the work of Ivanov et al. [31] briefly refers that the use of argon as carrier gas makes the process very inefficient and leads to films with poorer crystallinity.

Currently, the demand for fast and cost-efficient fabrication processes of high-quality materials and devices is on the agenda. Hence, an in-depth study of the feasibility of growing high quality epitaxial films of CrO_2 using argon as carrier gas becomes crucial, especially because of the well-known price difference between the two gases, with cost advantage to argon. Besides, argon is a more user-friendly gas. Therefore, the fact that the use of argon could eventually limit the CrO_2 synthesis reaction may be seen as a drawback to the envisaged scaling-up of the CrO_2 CVD process at an industrial level.

* Corresponding author. Departamento de Física, Faculdade de Ciências, Universidade de Lisboa, 1749-016 Lisboa, Portugal.
E-mail address: omconde@ciencias.ulisboa.pt (O. Conde).

This work reports on the synthesis and properties of CrO_2 thin films grown onto single crystal TiO_2 rutile substrates by CVD, using CrO_3 as chromium precursor and either oxygen or argon as carrier gas. A comparative study of the structural, microstructural and magnetic properties of the different films are presented.

2. Experimental details

The CrO_2 films were prepared in a tubular single-zone CVD furnace with independent control of the substrate temperature. Details of this setup were described in previous papers [28,29]. The thin films were grown onto TiO_2 (110) and TiO_2 (100) single crystal rutile substrates 0.5 mm thick and with 10×5 mm² surface area. Prior to their insertion into the reactor, the substrates were ultrasonically cleaned in organic solvents − acetone and isopropanol, rinsed in distilled water and dried with a N_2 flux. CrO_3 powder (purity 99.9%) was used as the precursor and either oxygen (purity 99.9992%) or argon (purity 99.9992%) as carrier gases. Films were grown at atmospheric pressure for deposition times varying between 10 and 240 min, using a gas flow rate of 150 sccm, a precursor temperature of 275 °C and a substrate temperature of 390 °C. In order to avoid the deposition of undesirable compounds during the initial stage of the deposition process, the substrate was heated up to the deposition temperature before the CrO_3 precursor attained its melting temperature (196 °C). Samples will be designated by A100, A110, O100 and O110 throughout the text, where A/O refers to argon/oxygen and 100/110 to the substrate orientation. Sometimes the deposition time, in minutes, is added to the sample's label (e.g. O110/180).

The surface morphology and microstructure of the films were analyzed using a JEOL 7001F scanning electron microscope with a field emission gun (FEG-SEM), and a Nanoscope IIIa multimode atomic force microscope (AFM) in tapping mode. Film thicknesses were evaluated by image digital processing of FEG-SEM cross-section micrographs. The crystallographic structure and phase composition of the as-grown films were studied by X-ray diffraction (XRD) with Cu Kα radiation, in the $\theta-2\theta$ coupled mode. The 2θ angular position and full-width at half-maximum (FWHM) of the diffraction lines were determined by fitting them with a Pseudo-Voigt function, after removing the Kα_2 contribution from the XRD patterns. The FWHM values were also corrected for the instrumental broadening. Phi-scan and rocking curve (RC) measurements were used to assess films epitaxiality and mosaicity. These studies were conducted on a Brücker-AXS D5000 diffractometer. Another diffractometer from Brücker-AXS (D8Discover) working with Cu Kα_1 radiation, an asymmetric two-bounce Ge (220) monochromator and a scintillation detector was used for recording the reciprocal space maps (RSM) and for carrying out the evaluation of the lattice parameters using the Bond method.

The magnetic properties of all the films were assessed at room temperature (RT) with longitudinal magneto-optical Kerr effect (MOKE) magnetometry. To observe the MOKE, the probing beam from a diode laser, operating at a wavelength of 670 nm with a power of 5.5 mW, was focused onto a ~50 μm diameter spot on the film surface using a 15 cm focal length lens.

3. Results and discussion

3.1. Structural data

The first set of results concerns XRD analysis of chromium oxide films grown on TiO_2 (110) substrates, using either oxygen or argon as carrier gas. This study is aimed at assessing the feasibility of CrO_2 growth under an argon atmosphere and, if the latter holds, at comparing film properties for both types of background gas phase.
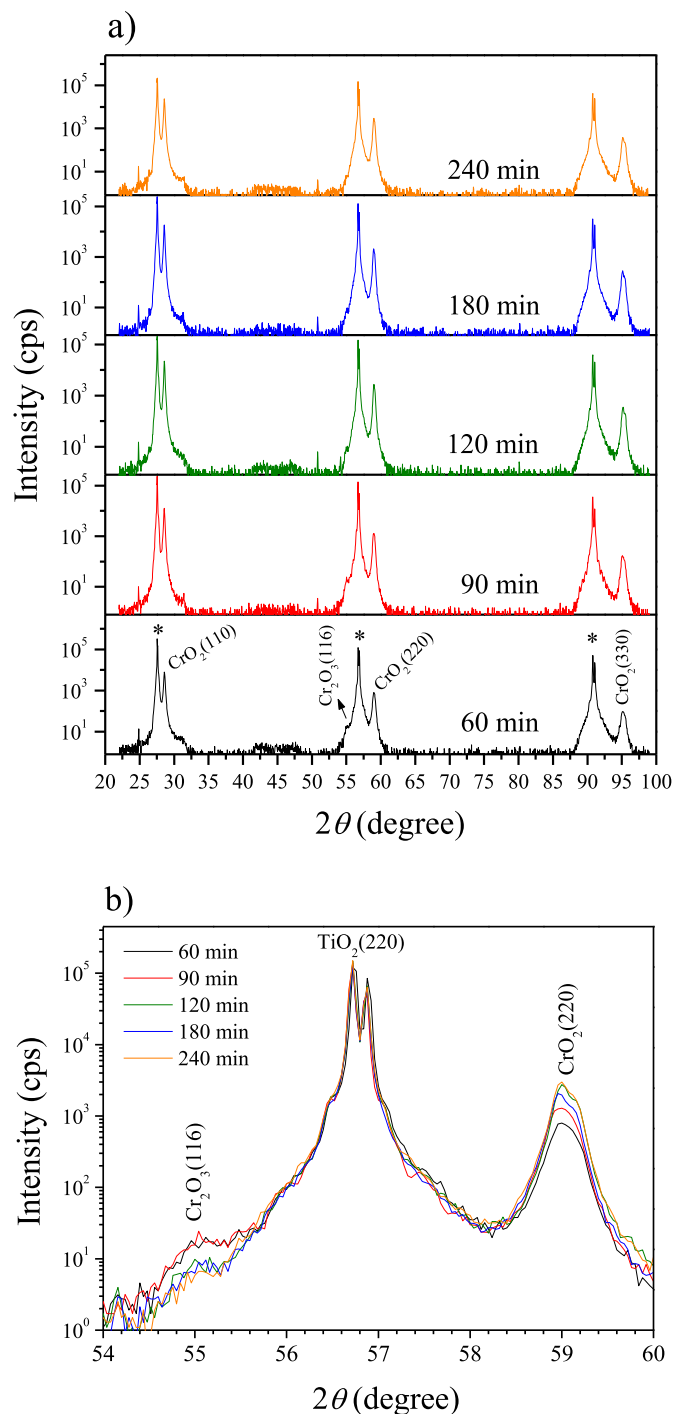
Of particular importance is to find out whether the presence of argon does or does not favour the occurrence of the antiferromagnetic Cr_2O_3 phase.

Fig. 1 shows the XRD patterns of films deposited at 390 °C with an oxygen flow rate of 150 sccm, for deposition times in the range of 60−240 min. All the patterns reveal diffraction peaks at $2\theta = 28.643°$, $2\theta = 59.096°$ and $2\theta = 95.335°$, which were identified as due to the (110), (220) and (330) reflections from CrO_2, respectively, by comparing with JCPDS file nº 9-332. The diffraction peaks labeled with the symbol (*) are attributed to the (110), (220) and (330) reflections from the rutile-TiO_2 substrate. No other phases are visible on this figure even if a logarithmic scale is used to plot the diffracted intensities. Similar patterns are displayed in Fig. 2a for the films deposited with argon substituting for oxygen as carrier gas. The growth parameters are identical for the two gases as well as the deposition times that were used. The same set of diffraction peaks related to the (110), (220) and (330) lattice planes of both CrO_2 film and rutile-TiO_2 substrate are displayed, however a low intensity extra peak may be observed on the low angle shoulder of the TiO_2 (220) line that can be assigned to the Cr_2O_3 (116) diffraction plane (JCPDS file nº 38-1479). This peak is clearly visible on an expanded $\theta-2\theta$ plot as that in Fig. 2b. It is present in all films as a very broad and low intensity peak indicating that the Cr_2O_3 formed phase is nanocrystalline and its amount is negligible. Nevertheless, the increase in intensity as the deposition time decreases, i.e. as the films become thinner, might be an indication that the Cr_2O_3 lies at the interface between the CrO_2 layer and the substrate.

The X-ray diffractograms of the films grown on TiO_2 (100) for a deposition time of 90 min are displayed in Fig. 3, for both types of carrier gas − oxygen and argon. Here, all the experimental parameters were maintained constant and assumed the same values
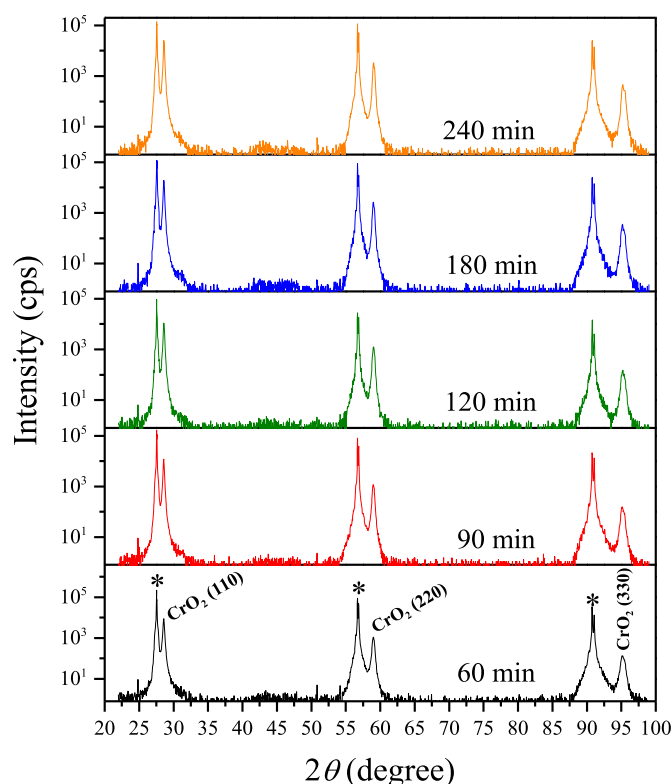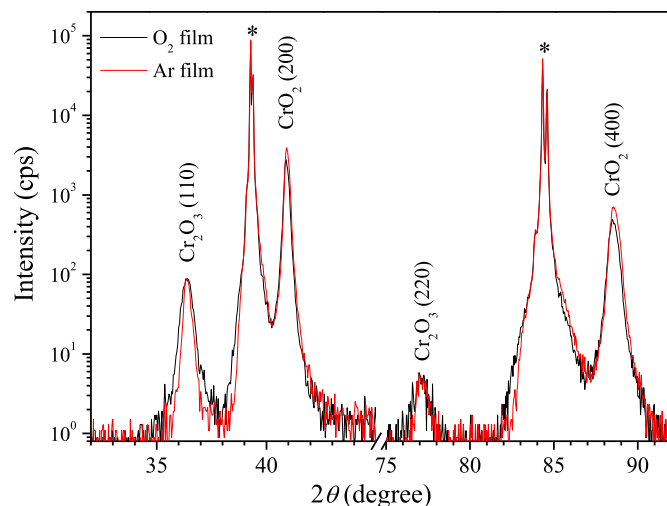

Fig. 1. X-ray diffractograms of O110-films grown at 390 °C with an oxygen flow rate of 150 sccm, for deposition times ranging from 60 to 240 min. The patterns show the (hh0) lines of CrO_2 while those labeled with * refer to the rutile-TiO_2 (110) single crystal substrate.

a)

b)

Fig. 2. a) X-ray diffractograms of A110-films grown at 390 °C with an argon flow rate of 150 sccm for deposition times ranging from 60 to 240 min. The patterns show the (hh0) lines of CrO_2 while those labeled with * refer to the rutile-TiO_2 (110) single crystal substrate; b) expanded plot in the 2θ: 54° − 60° region showing a broad and weak peak assignable to the (116) reflection from Cr_2O_3.
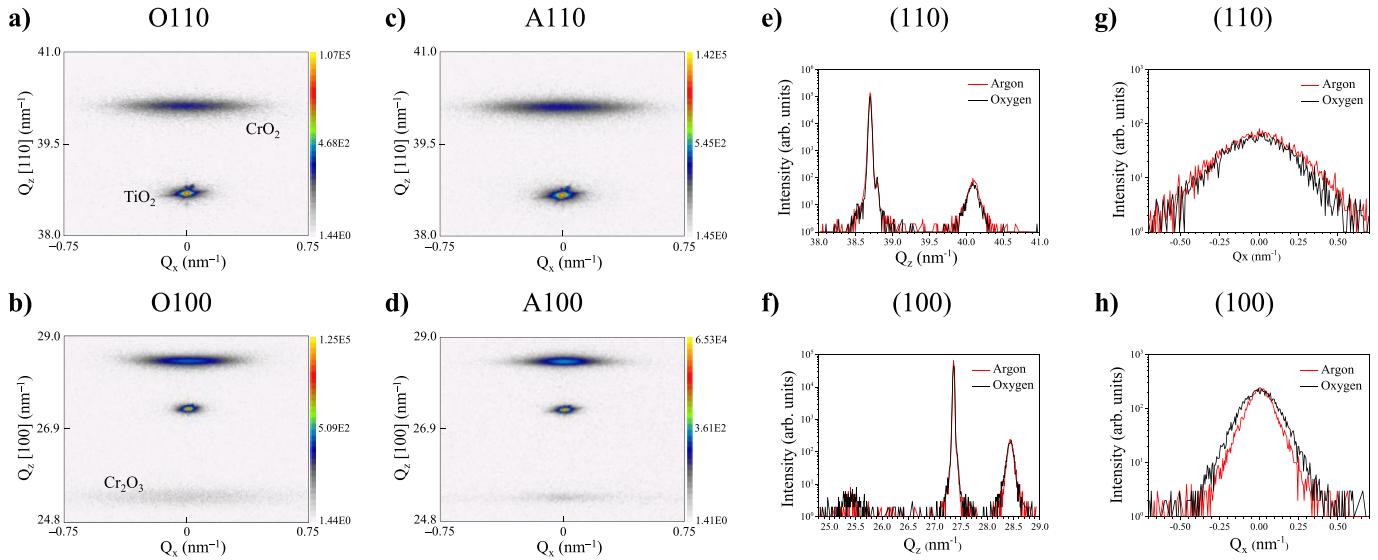

Fig. 3. XRD patterns of films deposited on TiO_2 (100) substrate using either argon or oxygen as carrier gas, for a deposition time of 90 min. The symbol (*) corresponds to substrate peaks. Both films were deposited with the gas flowing at 150 sccm and for a deposition temperature of 390 °C.

phase. This indicates that the Cr_2O_3 layer is textured and strongly correlated with the CrO_2 (100) − TiO_2 (100) system.

Indeed, it is well known that CrO_2 can grow epitaxially on TiO_2 substrates because both compounds adopt the same tetragonal rutile structure ($P4_2/mnm$) with a close match in lattice parameters: $a = b = 0.45933$ nm and $c = 0.29592$ nm for TiO_2, and $a = b = 0.44210$ nm and $c = 0.29160$ nm for CrO_2. Therefore, the lattice mismatch is −1.46% along the [001] direction (**c** axis) and −3.75% along either the [010] axis for TiO_2 (100) or the [$\bar{1}$10] direction for TiO_2 (110) substrate. In both cases CrO_2 films grow under interfacial tensile stress. Regarding the presence of the Cr_2O_3 layer in the films with (100) preferred orientation, it is expected that this layer will grow on top of CrO_2 since the surface area of the cells match to 99.4%, although 3 × 3 cells of CrO_2 are needed to fit one cell of Cr_2O_3, whereas the corresponding matching value for Cr_2O_3 directly grown on 3 × 3 TiO_2 (100) would be only 95.4%. It is believed that the Cr_2O_3 layer forms during the cooling of the samples inside the CVD reactor, from the deposition temperature of 390 °C down to room temperature. Using the method described in ref. [29], the thickness of this Cr_2O_3 top layer can be calculated. For instance, a value of 24.8 nm was obtained for the film A100/90, which represents 11.8% of the total film thickness.

In order to assess the crystalline quality of the films and possible structural misalignments between film and substrate, reciprocal space maps (RSM) were recorded around the (220) and (200) reflections of CrO_2 for the samples grown on TiO_2 (110) and TiO_2 (100), respectively. Fig. 4a−d displays typical symmetric RSMs for films of the different types although keeping the deposition time constant at 90 min. A qualitative inspection of these maps shows a strong coherence between the [110] axes of CrO_2 and TiO_2 in case of the (110) oriented substrate (Fig. 4a and c). For the (100) CrO_2/TiO_2 (Fig. 4b and d) a strong coherence is also observed not only between the [100] axis of both materials as well as the [110] axis of Cr_2O_3, which reinforces our previous statement on the structural relationship of the three compounds. Therefore, the following in-plane orientation epitaxial relationships can be written: $CrO_2(110)[110]\|TiO_2(110)[110]$ and $Cr_2O_3(110)[110]\|CrO_2(100)[100]\|TiO_2(100)[100]$.

An easy, rapid and accurate way of comparing these maps amongst themselves will consist of making vertical and horizontal cuts and plotting the intensities versus Qz (Fig. 4e and f) and Qx

as for the previous (110) oriented substrate. The CrO_2 layers grow with a (100) preferred orientation according to the orientation of the substrate and diffraction lines attributed to the (200) and (400) reflections of CrO_2, respectively at $2\theta = 40.855°$ and $2\theta = 88.491°$, and of TiO_2 were recorded. Besides these diffraction peaks, two other ones at $2\theta = 36.196°$ and $2\theta = 76.851°$ are clearly observed, which were indexed as (110) and (220) reflections from the Cr_2O_3

Fig. 4. Symmetric reciprocal space maps of films deposited with oxygen (panels a) and b)) and argon (panels c) and d)) onto rutile-TiO$_2$ substrates with (110) orientation (top) and (100) orientation (bottom). For all cases, deposition time is 90 min e), f): Vertical (Q$_z$) cut and g), h): Horizontal (Q$_x$) cut taken over the SRSMs shown in a) − d).
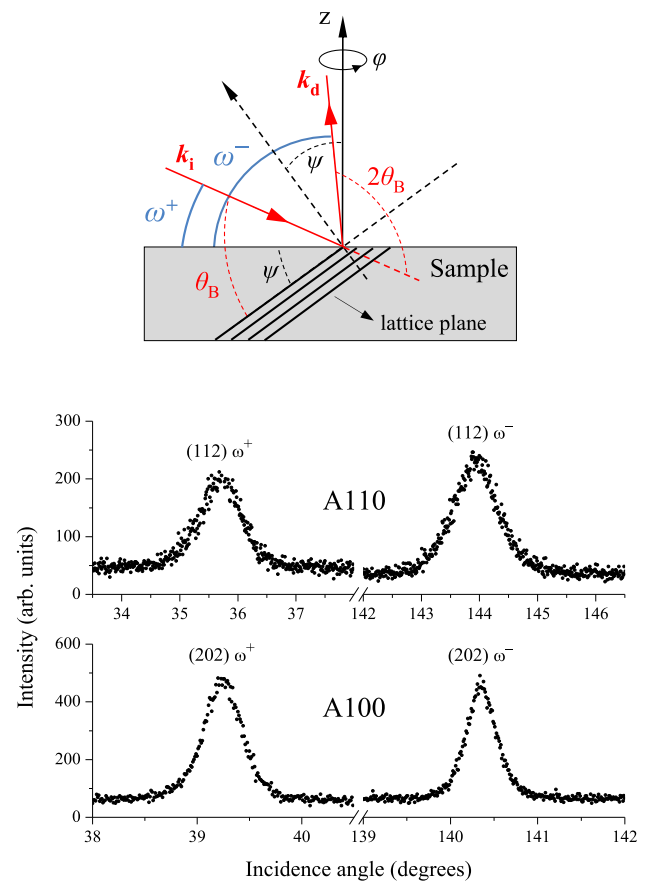
(Fig. 4g and h), respectively. The first plot gives the lattice parameter a for the films and substrates, determined from $a = 2\pi(h^2 + k^2)^{1/2}/Q_z$. The second plot is related to the crystalline quality of the CrO$_2$ layers, assessed through the analysis of the FWHM of the profiles. In general, the lines are broader (along Q$_x$) and thus a more pronounced mosaic structure is observed for the films grown under oxygen. This result agrees well with the rocking curves (not shown) measured around the (110) reflection, whose FWHM decreases from 1.2° down to 0.8° when deposition time increases from 60 to 240 min, the values for oxygen exceeding in general the argon ones. More striking is the difference of RC for both film orientations, for instance at t_{dep} = 90 min, we measured 1.0° and 0.5° for (110) and (100) films, respectively. Table 1 summarizes the Q$_z$ and lattice parameter a values for different samples. While the reproducibility is very high regarding the TiO$_2$ substrates, it is apparent that the CrO$_2$ films grown with (110) preferred orientation are under tensile stress (tensile strain <0.3%), assuming that a relaxed film will show a = 0.4421 nm. A calculated error of 2×10^{-4} nm is associated to the lattice parameter a of CrO$_2$.

Neither the $\theta-2\theta$ coupled diffraction nor the symmetric RSMs allow determining the c parameter. The lattice parameter c was determined with a high accuracy by using an XRD technique based on the Bond method [32,33] and the asymmetric reflections (112) and (202) respectively for (110) and (100) oriented substrates. It was assumed that $a = b$. We show on Fig. 5 an example of these measurements, and on Table 2 a summary of the results for selected samples. The calculated error associated to the lattice parameter c of CrO$_2$ is 3×10^{-5} nm. It comes out from these results that the structural parameters of CrO$_2$ films grown on TiO$_2$ substrates are

Fig. 5. Schematic configuration (top panel) for the measurement of the XRD asymmetric reflections by the Bond method, which are shown in the lower panel for two films grown with argon on (110) and (100) TiO$_2$ substrates.

not sensitive to the carrier gas used for film growth whether it is oxygen or argon. This is true for the (tensile or compressive) stress acting on the films as a result of lattice mismatch and/or difference in the thermal expansion coefficients of film and substrate. On the

Table 1
Q$_z$ cuts on the symmetrical RSM for the substrate and film, and determination of the lattice parameter a from the following equation: $a = 2\pi(h^2 + k^2)^{1/2}/Q_z$.

Sample	TiO$_2$ Q$_z$ (nm^{-1})	CrO$_2$ Q$_z$ (nm^{-1})	TiO$_2$ a (nm)	CrO$_2$ a (nm)
O110/180	38.699	40.102	0.45923	0.4432
A110/180	38.696	40.102	0.45926	0.4432
O110/90	38.697	40.091	0.45925	0.4433
A110/90	38.697	40.091	0.45925	0.4433
O100/90	27.360	28.440	0.45929	0.4419
A100/90	27.364	28.440	0.45923	0.4419

Table 2
Lattice parameters a and c of CrO_2 thin films, determined from symmetrical RSMs and Bond method, and tensile ($\varepsilon > 0$)/compressive ($\varepsilon < 0$) strain along the [100] and [001] crystallographic directions.

Sample	ω^+	ω^-	θ_B[a]	a (nm)[b]	c (nm)	$\varepsilon_{[100]} = \delta a/a$[c]	$\varepsilon_{[001]} = \delta c/c$[c]
O110/180 (112)	35.6662	143.9174	35.8744	0.4432	0.28094	2.49×10^{-3}	-3.65×10^{-2}
A110/180 (112)	35.6944	143.9389	35.8778	0.4432	0.28091	2.49×10^{-3}	-3.67×10^{-2}
O110/90 (112)	35.6560	143.9121	35.8674	0.4433	0.28099	2.71×10^{-3}	-3.64×10^{-2}
A110/90 (112)	35.6247	143.8528	35.8859	0.4433	0.28085	2.71×10^{-3}	-3.69×10^{-2}
O100/90 (202)	39.2620	140.3580	39.4520	0.4419	0.28998	-0.45×10^{-3}	-0.55×10^{-2}
A100/90 (202)	39.2445	140.3550	39.4448	0.4419	0.29000	-0.45×10^{-3}	-0.55×10^{-2}

[a] $\theta_B = [\omega^+ + (180 - \omega^-)]/2$.
[b] Value calculated in Table 1.
[c] $\varepsilon = \delta x/x = (x_{film} - x_{bulk})/x_{bulk}$.

other hand, the orientation of the substrate strongly influences the phase composition of the deposited material as well as the structural behaviour of the CrO_2 films. Indeed, it is clearly seen that while the films with (110) preferred orientation are compressively strained, those with (100) are almost fully relaxed, which allows to explain why their FWHM-RC are the lowest. This notorious influence of the substrate is in agreement with previous observations from other research groups however, while Anwar and Aarts [34] have found a similar behaviour to our films, Chetry et al. [35] and Pathak et al. [36] found the opposite and based their interpretation on differences in growth mode and morphology of the CrO_2 films. We will come back to this point in Section 3.3.

3.2. Film thickness and growth rate

The CrO_2 growth kinetics depends on a number of factors such as the geometry of the reactor, substrate material and crystallographic orientation, substrate and precursor temperatures, carrier gas, and carrier gas flow rate [28,29]. This section will focus on the role of the carrier gas on the thickness and growth rate of CrO_2 films for both types of single crystal substrates. Fig. 6 shows the thickness of CrO_2 films grown onto TiO_2 (110) as a function of deposition time for both oxygen and argon carrier gases. The inset of the figure shows the thickness of the films grown onto TiO_2 (100) for deposition times of 90 and 120 min. First of all, we notice that films grown with an oxygen flux are slightly thicker than those grown with an argon flux regardless of substrate orientation. Only at $t_{dep} = 240$ min is this trend reversed, which is probably related to

Fig. 6. Thickness vs. deposition time for CrO_2 films grown on TiO_2 (110) substrates with oxygen (full squares) and argon (full circles) carrier gases. The lines drawn are linear best fits. Inset: similar data for TiO_2 (100) substrate and deposition times of 90 and 120 min.

the faster consumption of the CrO_3 precursor when using oxygen carrier gas. Secondly, the thickness of films grown onto TiO_2 (100) is larger than that of films grown onto TiO_2 (110) by a factor of about 1.7–1.8. This value is slightly larger than the interplanar spacing ratio, $d_{100}/d_{110} = \sqrt{2}$, between (100) and (110) lattice planes of a tetragonal structure. Thus, the preferred growth orientation is in part responsible for the difference in thickness observed for the films grown on the two different substrates. Besides, the formation of a Cr_2O_3 layer on top of CrO_2 (100) films and different growth morphology (see below) can also be responsible for the observed thickness difference.
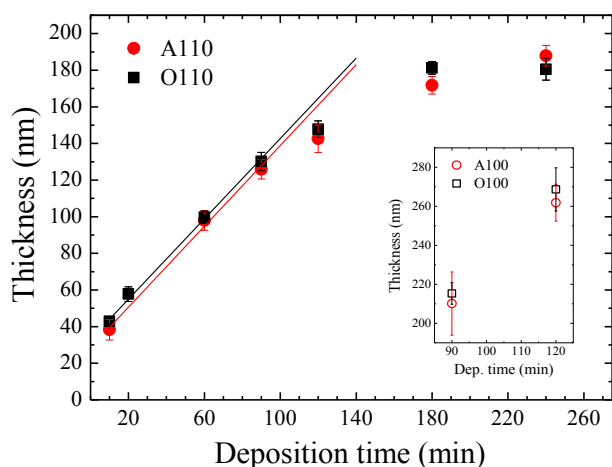
The thickness of CrO_2(110) films vs. deposition time (Fig. 6) shows two different regions − a linear region that extends up to ~100 min and a saturation region for deposition times greater than ~140 min. In the linear region, growth rates of 1.10 ± 0.04 nm and 1.10 ± 0.07 nm can be deduced for the films grown respectively with O_2 and Ar carrier gases. This result clearly shows that film growth is not influenced by which gas is used to transport the Cr precursor to the substrate. The observed transition from the linear stage to the saturation regime is due to a decrease of the Cr precursor concentration in the gas phase.

3.3. Morphology

The surface microstructure and morphology of the as-grown films was examined by FEG-SEM and AFM and is depicted in Fig. 7 for 90 min deposited films. Again, the type of background gas does not have a perceptible effect on film morphology and only the substrate orientation affects the film growth mode. For both types of substrates (and gases) similar CrO_2 building blocks consisting of rectangular shaped grains were observed. However, the way these grains pile up to grow a film varies with substrate orientation. For CrO_2 (100) the stacking of rectangular plates on top of each other with the same orientation is clearly observed on the AFM insets. This microstructural arrangement leaves low-density boundaries between the building blocks, or even voids, which allow explaining the smaller values of the FWHM-rocking curves, the almost absence of strain and rather smooth edges of the structures seen on the SEM images. On the contrary, for the CrO_2 (110) samples the piling-up of the rectangular platelets is not so perfect as previously and some misorientation exists, which leads to higher FWHM-RC values and denser structures with increased edges roughness. The root mean square surface roughness (R_q) measured on the insets (2×2 μm^2) of Fig. 7 took values within 2.8–3.9 nm and 5.4–6.5 nm respectively for CrO_2 (110) and CrO_2 (100), in agreement with the observed microstructures.

3.4. Magnetic measurements − coercivity

We have used longitudinal MOKE magnetometry with the applied magnetic field parallel to the easy axis (c-axis, oriented
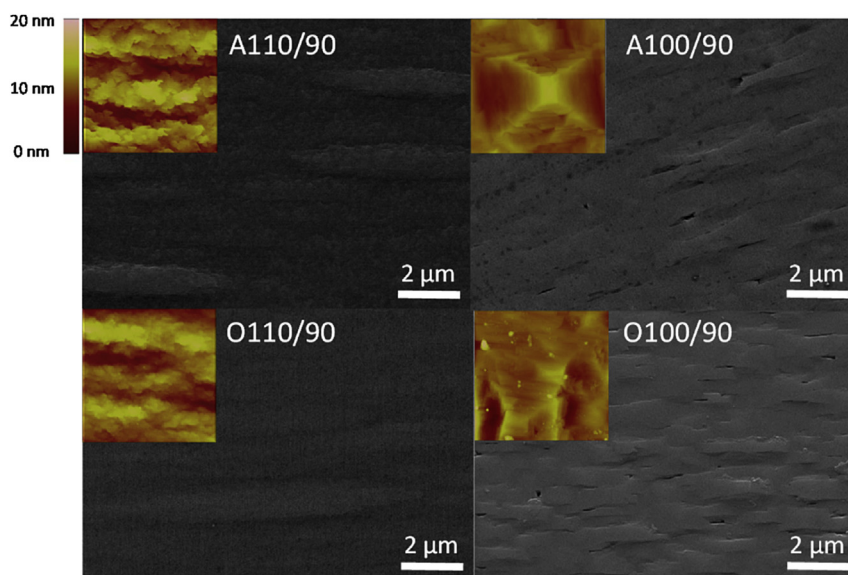
Fig. 7. FEG-SEM images of A100/90, O100/90, A110/90 and O110/90 CrO$_2$ films. Insets show the corresponding AFM images with 2 $\times$ 2 μm^2 and the same Z scale (0–20 nm).

along the larger side of the rectangular grains) to measure the room temperature magnetic properties of the as-deposited CrO$_2$ films on (110) and (100) TiO$_2$ substrates with oxygen and argon as carrier gases. Fig. 8 shows the hysteresis loops of samples deposited for 90 min, where it is observed an increase of $\leq$15% in maximum MOKE response when (110) substrate is replaced by the (100) one, under the same background gas. A similar increase is also observed for both substrates when oxygen is replaced by argon as flowing gas. On the contrary, a sharp reduction of ~60% in the switching field is observed for the (100) films grown during 90 min in comparison to the (110) ones. However, if the comparison is made between films of different orientation but the same thickness then the switching field reduces by ~40%. The carrier gas seems to have no remarkable influence on the coercive field. Various factors can contribute to the change of coercivity, such as stoichiometry deviation, grain size and strain [37]. Because Scherrer equation [38] applied to the analysis of the XRD peaks gives similar grain size for the films grown with either oxygen or argon, the highest strain

observed for the (110) films should be the main cause for their enhanced coercivity. On the other hand, structural imperfections, such as edge roughness, have been shown to alter the switching field of elongated structures [39], the coercivity increasing with the increase in edge roughness. For our films, the SEM and AFM images on Fig. 7 clearly show rough edges of the (110) elongated structures whereas the (100) blocks present sharp and smoother edges as discussed above in Section 3.3.

4. Conclusion

CrO$_2$ thin films were grown onto (110) and (100) TiO$_2$ rutile single crystal substrates by CVD using a highly efficient tubular single-zone CVD furnace with independent control of the substrate temperature. CrO$_3$ was used as chromium precursor and either O$_2$ or Ar as carrier gas. It is shown that the use of an Ar flux rather than an O$_2$ flux is not a limitation regarding the deposition of CrO$_2$. Instead, the use of argon carrier gas allows to grow high quality CrO$_2$ epilayers with similar structural, microstructural and magnetic properties of those grown with O$_2$ carrier gas. Also, the growth rate of the films does not depend on the carrier gas used. These results contrast with those reported by Ivanov et al., who mentioned [31] a low efficient growth process and poor quality films for argon assisted CVD CrO$_2$. For each type of carrier gas, the properties of the films are mainly determined by substrate orientation.

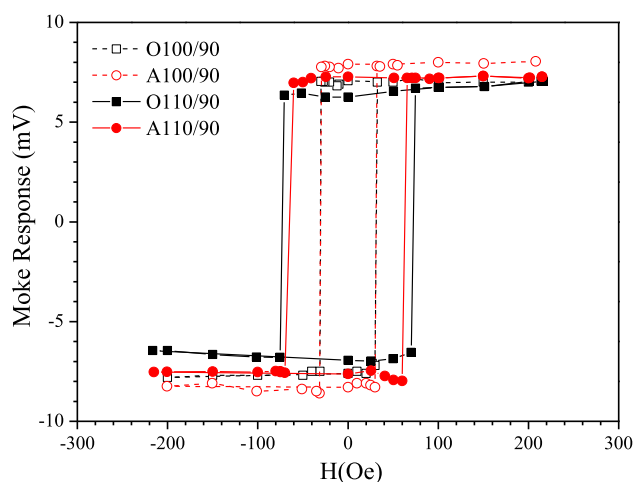**Fig. 8.** Hysteresis loops of CrO$_2$ films obtained by longitudinal MOKE magnetometry with the applied magnetic field parallel to the easy axis. Substrate orientation, deposition time, and carrier gas are indicated in the figure.

References

[1] H.Y. Hwang, S.-W. Cheong, Enhanced intergrain tunneling magnetoresistance in half-metallic CrO$_2$ films, Science 278 (1997) 1607–1609.
[2] L. Ranno, A. Barry, J.M.D. Coey, Production and magnetotransport properties of CrO$_2$ films, J. Appl. Phys. 81 (1997) 5774–5776.

[3] J.M.D. Coey, A.E. Berkowitz, L. Balcells, F.F. Putris, Magnetoresistance of chromium dioxide powder compacts, Phys. Rev. Lett. 80 (1998) 3815–3818.

[4] K. Suzuki, P.M. Tedrow, Resistivity and magnetotransport in CrO_2 films, Phys. Rev. B 58 (1998) 11597–11602.

[5] X.W. Li, A. Gupta, T.R. McGuire, P.R. Duncombe, G. Xiao, Magnetoresistance and Hall effect of chromium dioxide epitaxial thin films, J. Appl. Phys. 85 (1999) 5585–5587.

[6] A. Barry, J.M.D. Coey, M.A. Viret, CrO_2-based magnetic tunnel junction, J. Phys. Condens. Matter 12 (2000) L173–L175.

[7] M. Rabe, J. Dreβen, D. Dahmen, J. Pommer, H. Stahl, U. Rüdiger, G. Güntherodt, S. Senz, D. Hesse, Preparation and characterization of thin ferromagnetic CrO_2 films for applications in magnetoelectronics, J. Magn. Magn. Mater. 211 (2000) 314–319.

[8] W.J. DeSisto, P.R. Broussard, T.F. Ambrose, B.E. Nadgorny, M.S. Osofsky, Highly spin-polarized chromium dioxide thin films prepared by chemical vapor deposition from chromyl chloride, Appl. Phys. Lett. 76 (2000) 3789–3791.

[9] P.A. Stampe, R.J. Kennedy, S.M. Watts, S. von Molnár, Strain effects in thin films of CrO_2 on rutile and sapphire substrates, J. Appl. Phys. 89 (2001) 7696–7698.

[10] A. Anguelouch, A. Gupta, G. Xiao, D.W. Abraham, Y. Ji, S. Ingvarsson, C.L. Chien, Near-complete spin polarization in atomically-smooth chromium-dioxide epitaxial films prepared using a CVD liquid precursor, Phys. Rev. B 64 (2001), 180408(R).

[11] U. Rüdiger, M. Rabe, K. Samm, B. Özyilmaz, J. Pommer, M. Fraune, G. Güntherodt, S. Senz, D. Hesse, Extrinsic and intrinsic magnetoresistance contribuitions of CrO_2 thin films, J. Appl. Phys. 89 (2001) 7699–7701.

[12] Y.S. Dedkov, M. Fonine, C. König, U. Rüdiger, G. Güntherodt, Room-temperature observation of high-spin polarization of epitaxial CrO_2 (100) island films at the Fermi energy, Appl. Phys. Lett. 80 (2002) 4181–4183.

[13] V.A. Jaleel, T.S. Kannan, Hydrothermal synthesis of chromium dioxide powders and their characterization, Bull. Mater. Sci. 5 (1983) 231–246.

[14] R.S. Keizer, S.T.B. Goennenwein, T.M. Klapwijk, G. Miao, G. Xiao, A. Gupta, A spin triplet supercurrent through the half-metallic ferromagnet CrO_2, Nature 439 (2006) 825–827.

[15] M.S. Anwar, M. Veldhorst, A. Brinkman, J. Aarts, Long range supercurrents in ferromagnetic CrO_2 using a multilayer contact structure, Appl. Phys. Lett. 100 (2012) 052602.

[16] K.A. Yates, W.R. Branford, F. Magnus, Y. Miyoshi, B. Morris, L.F. Cohen, P.M. Sousa, O. Conde, A.J. Silvestre, The spin polarization of CrO_2 revisited, Appl. Phys. Lett. 91 (2007) 172504.

[17] A. Singh, S. Voltan, K. Lahabi, J. Aarts, Colossal proximity effect in a superconducting triplet spin valve based on the half-metallic ferromagnet CrO_2, Phys. Rev. X 5 (2015) 021019.

[18] W.R. Branford, K.A. Yates, E. Barkhoudarov, J.D. Moore, K. Morrison, F. Magnus, Y. Miyoshi, P.M. Sousa, O. Conde, A.J. Silvestre, L.F. Cohen, Coexistence of universal and topological anomalous hall effects in metal CrO_2 thin films in the dirty limit, Phys. Rev. Lett. 102 (2009) 227201.

[19] Y. Ding, C. Yuan, Z. Wang, S. Liu, J. Shi, R. Xiong, D. Yin, Z. Lu, Improving thermostability of CrO_2 thin films by doping with Sn, Appl. Phys. Let. 105 (2014) 092401.

[20] K.G. West, M. Osofsky, I.I. Mazin, N.N.N. Dao, S.A. Wolf, J. Lu, Magnetic properties and spin polarization of Ru doped half metallic CrO_2, Appl. Phys. Let. 107 (2015) 12402.

[21] I.V. Solovyev, I.V. Kashin, V.V. Mazurenko, Mechanisms and origins of half metallic ferromagnetism in CrO_2, Phys. Rev. B 92 (2015) 144407.

[22] S. Mironov, A. Buzdin, Triplet proximity effect in superconducting heterostructures with a half metallic layer, Phys. Rev. B 92 (2015) 184506.

[23] M. Shima, T. Tepper, C.A. Ross, Magnetic properties of chromium oxide and iron oxide films produced by pulsed laser deposition, J. Appl. Phys. 91 (2002) 7920–7922.

[24] N. Popovici, M.L. Paramês, R.C. Silva, O. Monnereau, P. Sousa, A.J. Silvestre, O. Conde, KrF pulsed laser deposition of chromium oxide thin films from Cr_8O_{21} targets, Appl. Phys. A 79 (2004) 1409–1411.

[25] D. Stanoi, G. Socol, C. Grigorescu, F. Guinneton, O. Monnereau, L. Tortet, T. Zhang, I.N. Mihailescu, Chromium oxides thin films prepared and coated in situ with gold by pulsed laser deposition, Mater. Sci. Eng. B 118 (2005) 74–78.

[26] X.W. Li, A. Gupta, G. Xiao, Influence of strain on the magnetic properties of epitaxial (100) chromium dioxide (CrO_2) films, Appl. Phys. Lett. 75 (1999) 713–715.

[27] M. Rabe, J. Pommer, K. Samm, B. Özyilmaz, C. König, M. Fraune, U. Rüdiger, G. Güntherodt, S. Senz, D. Hess, Growth and magnetotransport study of thin ferromagnetic CrO_2 films, J. Phys. Condens. Matter 14 (2002) 7–20.

[28] P.M. Sousa, S.A. Dias, A.J. Silvestre, O. Conde, B. Morris, K.A. Yates, W.R. Branford, L.F. Cohen, CVD of CrO_2: towards a lower temperature deposition process, Chem. Vap. Depos. 12 (2006) 712–714.

[29] P.M. Sousa, S.A. Dias, O. Conde, A.J. Silvestre, W.R. Branford, B. Morris, K.A. Yates, L.F. Cohen, Influence of growth temperature and carrier flux on the structure and transport properties of highly oriented CrO_2 on Al_2O_3 (0001), Chem. Vap. Depos. 13 (2007) 537–545.

[30] C. Aguilera, J.C. González, A. Borrás, D. Margineda, J.M. González, A.R. González-Elipe, J.P. Espinós, Preparation and characterization of CrO_2 films by low pressure chemical vapor deposition from CrO_3, Thin Solid Films 539 (2013) 1–11.

[31] P.G. Ivanov, S.M. Watts, D.M. Lind, Epitaxial growth of CrO_2 thin films by chemical-vapor deposition from a Cr_8O_{21} precursor, J. Appl. Phys. 89 (2001) 1035–1040.

[32] W.L. Bond, Precision lattice constant determination, Acta Cryst. 13 (1960) 814–818.

[33] N. Herres, L. Kirste, H. Obloh, K. Koehler, J. Wagner, P. Koidl, X-ray determination of the composition of partially strained group-III nitride layers using the extended Bond method, Mater. Sci. Eng. B 91–92 (2002) 425–432.

[34] M.S. Anwar, J. Aarts, Inducing supercurrents in thin films of ferromagnetic CrO_2, Supercond. Sci. Technol. 24 (2011) 024016.

[35] K.B. Chetry, M. Phatak, P. LeClair, A. Gupta, Structural and magnetic properties of (100)- and (110)-oriented epitaxial CrO_2 films, J. Appl. Phys. 105 (2009) 083925.

[36] M. Phatak, H. Sato, X. Zhang, K.B. Chetry, D. Mazumdar, P. LeClair, A. Gupta, Substrate-induced strain and its effect in CrO_2 thin films, J. Appl. Phys. 108 (2010) 053713.

[37] N. Li, A.Y.-H.A. Wang, N.M. Iliev, T.M. Klein, A. Gupta, Growth of atomically smooth epitaxial nickel ferrite films by direct liquid injection CVD, Chem. Vap. Depos. 17 (2011) 261–269.

[38] B.D. Cullity, S.R. Stock, Elements of X-ray Diffraction, third ed., Prentice Hall, New Jersey, 2001, p. 170.

[39] M.T. Bryan, D. Atkinson, R.P. Cowburn, Edge roughness and coercivity in magnetic nanostructures, J. Phys. Conf. Ser. 17 (2005) 40–44 and references therein.